Effects of Chemical Curing on the Properties of Wood-based Precursors and Activated Carbon Microspheres

Junbo Shang,[a,b] Jian Lin,[a,b,*] and Guangjie Zhao [a]

Wood-based precursors and activated carbon microspheres were prepared through chemical curing and activation. The effects of the hydrochloric acid concentration on the thermal stability of the precursors and pore structures of the wood-based activated carbon microspheres were studied by thermo-gravimetric analysis, Fourier transform infrared spectroscopy, scanning electron microscopy, X-ray photoelectron spectroscopy, and analysis of the specific surface area and pore structure. The results showed that the reaction between the carbocations and benzene rings contributed to an increase in the methylene bonds, which reinforced the cross-linking degree and thermal stability of the wood-based cured microspheres. After activation, a typical microporous structure and part of an irregular mesoporous structure were formed in the wood-based activated carbon microspheres. The specific surface area, micropore volume, and mesopore volume increased, reaching maximum values of 1551 m^2/g, 0.506 cm^3/g, and 0.246 cm^3/g at 4 mol/L hydrochloric acid, respectively, and then decreased as the hydrochloric acid concentration increased. The pore size distributions of the micropore and mesopore areas were in the range of 0.5 nm to 1.4 nm and 2 nm to 10 nm, respectively.

Keywords: Chemical curing; Wood; Thermal stability; Pore structure; Activated carbon microspheres

*Contact information: a: Beijing Key Laboratory of Wood Science and Engineering, Beijing Forestry University, Beijing 100083, China; b: MOE Key Laboratory of Wooden Material Science and Application, Beijing Forestry University, Beijing 100083, China; *Corresponding author: linjian0702@bjfu.edu.cn*

INTRODUCTION

Activated carbon microspheres have been widely used in many areas, such as supercapacitors (Wang *et al*. 2014), gas adsorption (Wickramaratne and Jaroniec 2013), and biological medicine (Ye *et al*. 2008), because of advantages such as its smooth surface, high packing density, high mechanical strength, good uniformity, rolling property, and low flow resistance (Shen *et al*. 2008). Generally, most raw materials used for activated carbon microspheres are derived from fossil resources, such as pitch, coal, and phenolic resin. Environmental concerns have prompted researchers to seek alternative materials for the preparation of activated carbons from biomass materials, such as wood (Wang *et al.* 2015), bamboo (Ma *et al*. 2014), lignin (Lin and Zhao 2016), hemp (Geng *et al.* 2017), *etc*. Wood and wood wastes are a huge source of raw materials for the preparation of activated carbon materials. Based on the liquefaction of wood, precursors are prepared without complicated separation and purification processes, and wood-based carbon fibers can be successfully produced (Ma and Zhao 2011). The tensile strength of wood-based carbon fibers is almost the same as that of pitch-based carbon fibers (Li and Ma 2013).

However, further research has demonstrated that liquefied wood is more suitable for preparing porous structural carbon materials by physical (Liu *et al.* 2015) or chemical

activation (Huang and Zhao 2016). The preparation processes for wood-based activated carbon fibers from liquefied wood include wood liquefaction, melt spinning, chemical curing, carbonization, and activation. Before activation, the process of chemical curing is a key step to improve the thermal stability of the precursors (Lin *et al.* 2013). In addition to treatment with air or oxygen for the preparation of polyacrylonitrile-based (PAN-based) carbon fibers, chemical curing requires a mixed solution of hydrochloric acid and formaldehyde to stabilize the primary fibers. The process begins with immersing primary fibers in a curing solution under the conditions of heating and incubation (Ma and Zhao 2008). During the chemical curing process, formaldehyde molecules in a solution, *i.e.*, carbocations, react and form into methylene in the benzene rings of the primary fibers, which results in a three-dimensional network structure between the molecular chains. Therefore, the thermal-fusible primary fibers are transformed into thermal-setting precursors to prevent melting during carbonization and activation (Lin *et al.* 2012).

In this study, wood-based activated carbon microspheres (WACMCs) were successfully obtained from liquefied wood microspheres (LWMs) through the preparation of microspheres, chemical curing, carbonization, and activation. The thermal decomposition and chemical structure of the precursors prepared by chemical curing were analyzed by thermo-gravimetric analysis (TGA) and Fourier transform infrared (FTIR) spectroscopy. The morphologies were studied with scanning electron microscopy (SEM). The surface chemical composition was examined using an X-ray photoelectron spectrometer. The N_2 adsorption/desorption isotherms and pore volumes were measured with a specific surface area and porosity analyzer.

EXPERIMENTAL

Materials

Chinese fir (*Cunninghamia lanceolata*) was obtained from Fujian province, China. The chemicals, including phenol, phosphoric acid, hexamethylenetetramine (HTMA), hydrochloric acid, and polyvinyl alcohol (PVA), were purchased from Beijing Lanyi Chemical Products Corp. (Beijing, China). All of the chemicals were used directly without further purification.

Methods

Preparation of the precursors

A mixture of 25 g of dried Chinese fir powder (20 mesh to 80 mesh) and 100 g of phenol was put into a bottle flask, and 8 g of phosphoric acid (8% based on the weight of the phenol) were added. The flask was immersed in an oil bath, heated rapidly from room temperature to 160 °C, and incubated for 2.5 h. The flask was then cooled to room temperature with cool water, and the resultant mixture was filtered through a glass crucible filter (G2, pore diameter of 10 μm to 15 μm) to separate the filtrate from the residue (Shang *et al.* 2015). Subsequently, the filtered residue was put into a solution pre-heated to 65 °C with 6% PVA (based on the weight of the liquefied wood) and stirred at 400 rpm for 2 h. Then, the LWMs were obtained by washing the resultant mixture with distilled water and drying them in a vacuum oven at 45 °C for 24 h. The wood-based cured microspheres (LWCMs) were obtained by immersing the LWMs in a solution of hydrochloric acid (molar concentrations of 1 mol/L, 2 mol/L, 3 mol/L, 4 mol/L, 5 mol/L, and 6 mol/L) and 5 g/L HTMA, which was incubated at 85 °C for 2 h. Then, the resultant mixture was washed

with distilled water and dried in a vacuum oven (degree of vacuum = 0.1 MPa) at 45 °C. The samples were marked as LWCM-x, where x is the molar concentration.

Preparation of the wood-based activated carbon microspheres

The LWCMs were carbonized at 600 °C at a heating rate of 4 °C/min under N_2, and were incubated for 1 h. Then, the temperature was increased from 600 °C to 800 °C at a heating rate of 4 °C/min, and they were incubated for 1 h under N_2 and water steam. The WACMCs were obtained and marked as WACMC-x, where x is the molar concentration.

Characterization

Thermo-gravimetric analysis

The weight loss behaviors and decomposition temperatures of the samples were determined using a TGA device (TGA STA449F3, Netzscn Corp., Selb, Germany) from room temperature to 600 °C at a heating rate of 10 °C/min in high-purity argon steam (flow rate of 60 mL/min).

Fourier transform infrared spectroscopy

Fourier transform infrared spectroscopy of the samples was performed using a FTIR spectrophotometer (Tensor 27, Bruker Corp., Karlsruhe, Germany). The survey resolution was 4 cm^{-1} with 32 scans and a scanning range of 4000 cm^{-1} to 500 cm^{-1}. The samples were dried before they were mixed with water-removed KBr crystals, and then were ground in an agate mortar at a weight ratio of 1:100 (sample to KBr crystals). A few samples were put on a tablet press (FW-4A, Ruilaite Corp., Tianjing, China) to make a transparent sheet for the measurements.

Scanning electron microscopy

The morphologies of the samples were observed with SEM (S-3400N, Hitachi, Tokyo, Japan) after a gold-coated treatment (E-1010, Hitachi) at magnification factors of 1500x and 2000x and an accelerating voltage of 10 kV.

X-ray photoelectron spectroscopy

The X-ray photoelectron spectroscopy (XPS) measurements were performed on a spectrophotometer (ESCALAB 250Xi, Thermo Fisher Scientific Inc., MA, USA) to determine the quantity and type of functional groups present on the surface of the samples with a monochromated Al Kα X-ray source ($h\nu$ = 1486.6 eV). The survey scans were collected from the binding energy range of 0 eV to 1350 eV. A nonlinear, least squares regression analysis program (XPSPEAK software, Version 4.1, Informer Technologies, Inc., Hong Kong, China) was used for the XPS spectral deconvolution.

Specific surface area and pore structure analysis

The samples were out-gassed at 300 °C for 3 h to remove any moisture or volatile compounds within the pores of the samples. The N_2 adsorption-desorption isotherms were then measured at 77 K with a specific surface area and porosity analyzer (Autosorb-IQ, Quantachrome Instruments Corp., Florida, USA). The Brunauer-Emmett-Teller (BET) model was used to calculate the specific surface area (S_{BET}) from the N_2 adsorption isotherms in the relative pressure (P/P_0) range of 0.05 to 0.3 (Okada *et al.* 2003). The adsorption total pore volumes at relative pressures of 0.1 and 0.995 are equal to the volume of the micropores and total volume of the micropores and mesopores (V_{tot}), respectively

(Azargohar and Dalai 2008). The micropore (S_{micro}) and mesopore (S_{meso}) areas were calculated according to the t-plot and Barrett-Joyner-Halenda methods, respectively (De Boer *et al.* 1966; Valente Nabais *et al.* 2004; Li and Ma 2013). The pore size distribution was calculated using the quenched solid density functional theory method (Lastoskie *et al.* 1993; Neimarka *et al*. 2009).

RESULTS AND DISCUSSION

Thermal Stability of the LWM and LWCMs

Figure 1 shows the thermo-gravimetric (TG) and differential thermo-gravimetric (DTG) curves of the LWM and LWCMs prepared at different hydrochloric acid concentrations.

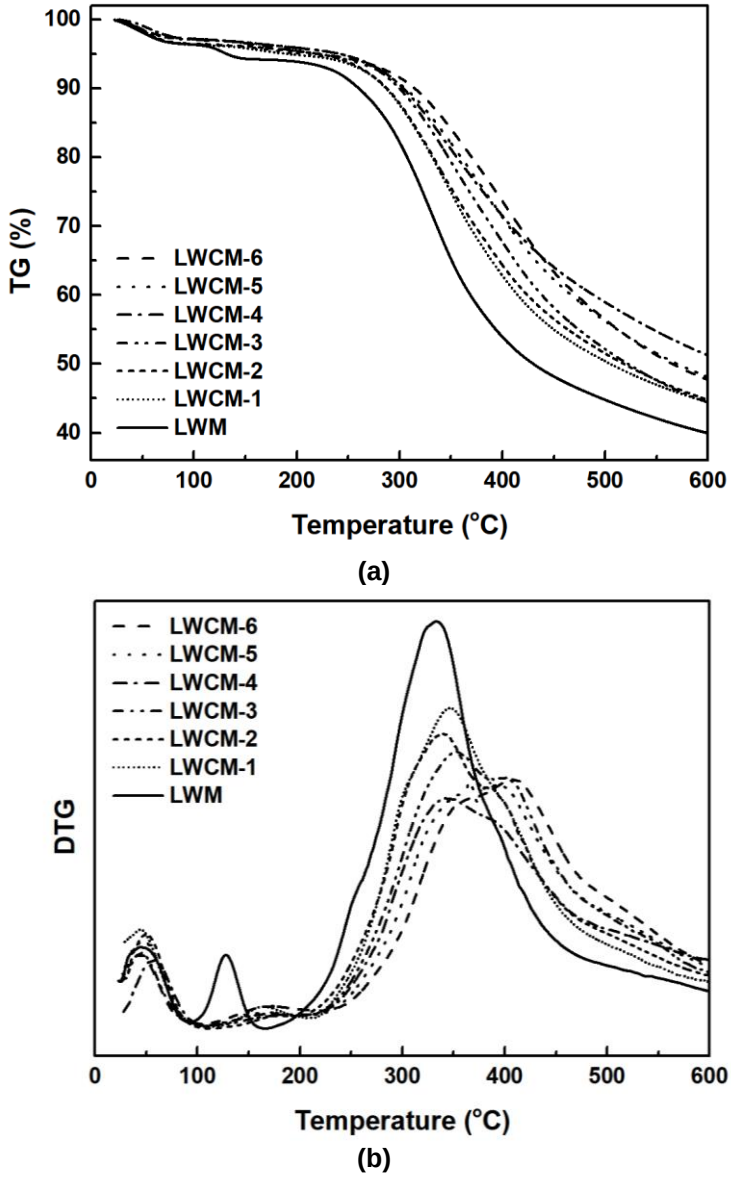

Fig. 1. TG (a) and DTG (b) curves of the LWM and LWCMs prepared at various hydrochloric acid concentrations

Figure 1a shows that the trends of the TG curves from room temperature to 100 °C were similar, and the pyrolysis weight loss of all the samples was less than 5%, which was mainly because of the removal of water. However, as the pyrolysis temperature increased, the difference in the pyrolysis weight loss between the LWM and LWCMs increased. From 100 °C to 220 °C, the pyrolysis weight loss of the LWM appeared to decrease and the DTG curve showed an obvious peak at approximately 120 °C, which is shown in Fig. 1b. In contrast, there was a small decrease for the LWCMs because of the small quantity of small molecules that escaped after chemical curing.

When the pyrolysis temperature was above 200 °C, there was a remarkable variation in the TG curves. Thermal decomposition and combustion took place between 200 °C to 600 °C, and byproducts, such as small molecular weight substances like CH_4, CO, and CO_2, were combusted or evaporated (Zhang and Shen 2009). Accompanied with an increase in the hydrochloric acid concentration, the pyrolysis reaction rate decreased as the DTG curves of the LWCMs became wider. Moreover, the peak temperature of the maximum pyrolysis reaction rate increased. The highest pyrolysis peak temperature of the LWCMs was 406 °C for the sample treated with 6 mol/L hydrochloric acid, which was 73 °C higher than that of the LWM (333 °C). These results indicated that the cross-linking degree and thermal stability of the precursors were improved by chemical curing (Ma and Zhao 2008).

During the chemical curing process, carbocations were generated from the reaction of the hydrochloric acid and HTMA. The more hydrochloric acid was added, the more carbocations were generated in the solution. When the LWCMs were immersed in the curing solution, carbocations diffused into the interior of the LWCMs and promoted the uniformity of the cross-linking degree of the LWCMs from the inside to the outside. When the pyrolysis temperature increased to 600 °C, the pyrolysis residual ratio of the LWM was below 40%. As the hydrochloric acid concentrations of the LWCMs were increased from 1 mol/L to 6 mol/L, the pyrolysis residual ratio first increased and then decreased. The highest pyrolysis residual ratio of the LWCMs was 51.3%, which occurred in the solution with a hydrochloric acid concentration of 4 mol/L, higher than that of 47.8% (the hydrochloric acid concentration of 6 mol/L).

An increase in the hydrochloric acid concentration increased the amount of carbocations in the solution and enhanced the cross-linking degree of the molecular chain of the LWCMs. However, an excessive hydrochloric acid concentration made the reaction occur too quickly, so that the surface layer of the precursors was cured immediately and became denser as the reaction continued. Therefore, the carbocations were prevented from penetrating into the precursors to fortify the cross-linking structures inside, which resulted in a low cross-linking degree and thermal stability (Ma and Zhao 2010). In contrast, when the hydrochloric acid concentration was too low, the deficient amount of carbocations was unable to support enough curing reactions with the precursors, which resulted in a vulnerable cross-linking structure and poor thermal stability.

The morphologies of the LWM and LWCM-4 are depicted in Fig. 2. Although there was no difference in the sphericity between the two samples, the chemical curing process formed a dense solidified layer on the surface of the LWCM-4 and the surface was denser than that of the LWM (Zhang and Shen 2009). Beneath the surface layer, the porous structures of the LWM and LWCM-4 were observed clearly. Therefore, the LWCM-4 acquired a dense surface layer outside and a rich porous structure inside, and further processes, such as carbonization and activation, are necessary to open up the inner and outer pore connection.

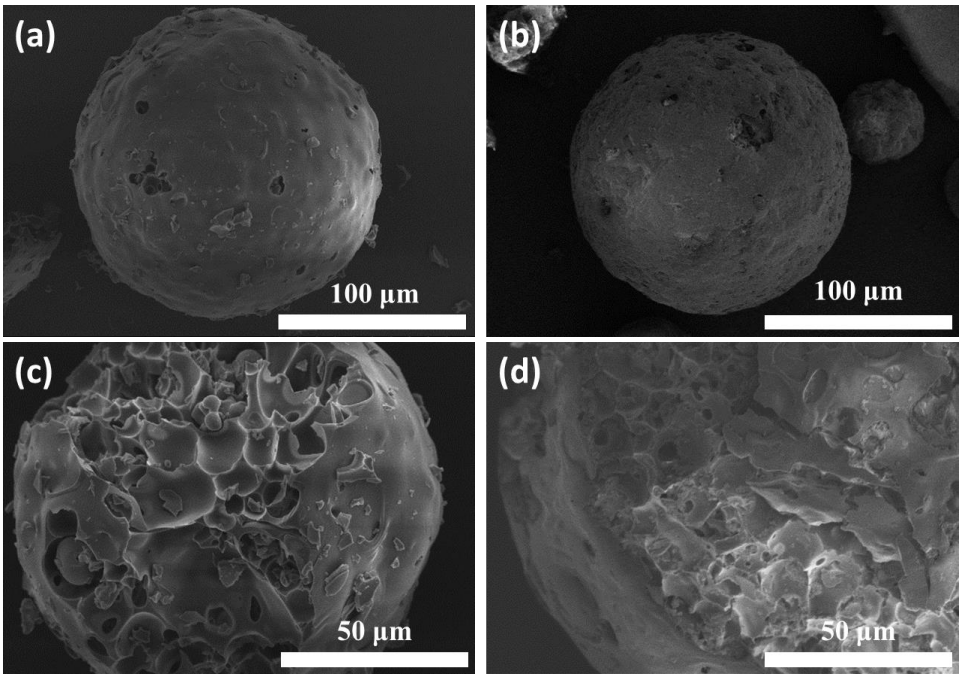

Fig. 2. SEM images of the LWM (a) and LWCM-4 (b) at 500x magnification and the LWM (c) and LWCM-4 (d) at 1000x magnification

Cross-linking Reaction during Chemical Curing

Figure 3 shows the FTIR spectra of the LWM and LWCMs prepared at different hydrochloric acid concentrations. During the process of chemical curing, the reaction between the carbocations and reactive carbon of the benzene rings in the precursors was attributed to the generation of methylene groups, cross-linking of the molecular chains, and formation of three dimensional structures (Shang *et al.* 2015). When the hydrochloric acid concentration increased, the absorption peaks from 3430 cm^{-1} to 3400 cm^{-1} (stretching vibration of hydroxyl groups), 1610 cm^{-1}, and 1454 cm^{-1} (stretching vibration of C=C in aromatic rings) weakened at first and then were enhanced, which indicated that dehydration condensation reactions occurred between the phenolic hydroxyl groups and carbocations from the curing solution.

Carbocations were generated from the HTMA under acidic conditions, and the lignin structural units were connected in the form of methylene bonds to develop a cross-linked structure, which fortified the thermal stability of the LWCMs. The intensity of the absorption peak at 2932 cm^{-1} (stretching vibration of methylene groups) first increased and then decreased, whereas the intensities of the absorption peaks at 1099 cm^{-1} (aromatic ether bonds) and 1029 cm^{-1} (hydroxyl methyl groups) decreased at first and then increased. This demonstrated that the aromatic ether bonds and hydroxyl methyl groups were converted into methylene bonds and the cross-linked structure of the precursors was enhanced (Shang *et al.* 2015). Meanwhile, the absorption peaks at 880 cm^{-1} and 823 cm^{-1} decreased at first and then increased as the hydrochloric acid concentration increased, which indicated that the dehydration condensation reactions between the carbocations and active atomic hydrogen of the benzene rings also formed cross-linked structures during chemical curing.

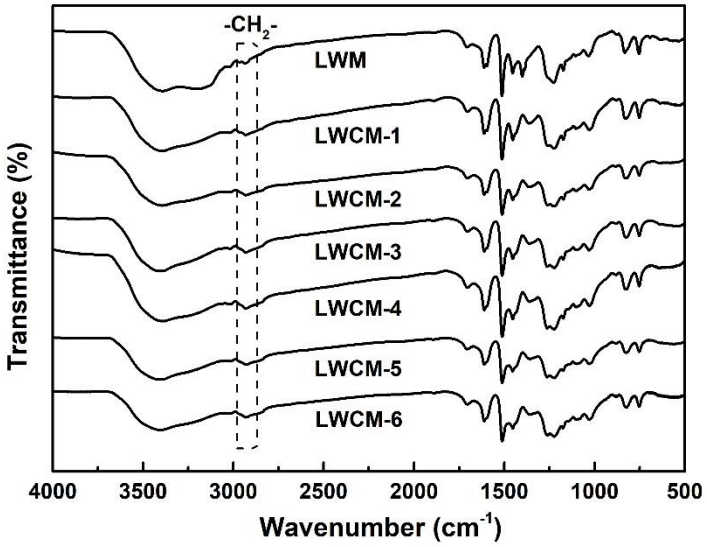

Fig. 3. FTIR spectra for the LWM and LWCMs prepared at various hydrochloric acid concentrations

The activity of the carbocations became stronger as the hydrochloric acid concentration increased, which resulted in a dense solidified layer on the surface of the LWCMs. The carbocations were prevented from continuously entering into the interior, which led to an inconsistent cross-linked structure. Therefore, the LWCMs prepared at the hydrochloric acid concentration of 4 mol/L showed a suitable curing rate and higher degree of cross-linking, which contributed to better thermal stability (Ma and Zhao 2008). These results were consistent with the variations in the TG and DTG curves (Fig. 1).

Variation in the Chemical Compositions for the Different Processes

The XPS spectra of the LWM, LWCM-4, and WACMC-4 are depicted in Fig. 4a. Table 1 summarizes the elemental compositions on the surface of these samples. The elemental contents of the LWM and LWCM-4 were similar, mainly because the chemical curing was a process that formed methylene bonds and the quantity of elemental nitrogen introduced from the HTMA was small.

After activation, the content of elemental carbon increased to over 95% and the oxygen content was reduced to 4.35%. A large amount of carbon and oxygen was combusted or evaporated from the oxygen-containing functional groups. Consequently, the elemental carbon was enriched, and oxygen and nitrogen escaped as byproducts (Mangun *et al.* 2001).

The C1s spectra for the LWM, LWCM-4, and WACMC-4 were similar. Therefore, only the spectrum of the WACMC-4 is depicted in Fig. 4b. For all of the samples, the C1s signals showed an asymmetric tailing, which was attributed to the intrinsic asymmetry of the graphite peaks and contribution of oxygen surface complexes. Deconvolution of the four individual component peaks of the C1s spectra was done and indicated the presence of graphitic carbon (284.6 eV to 284.8 eV); carbon present in alcohol, ether, or C=N groups (285.5 eV to 286.2 eV); carbonyl or quinine groups (286.4 eV to 287.1 eV); and carboxyl, lactone, or ester groups (288.1 eV to 288.9 eV) (Chiang *et al.* 2007; Liu and Zhao 2012).

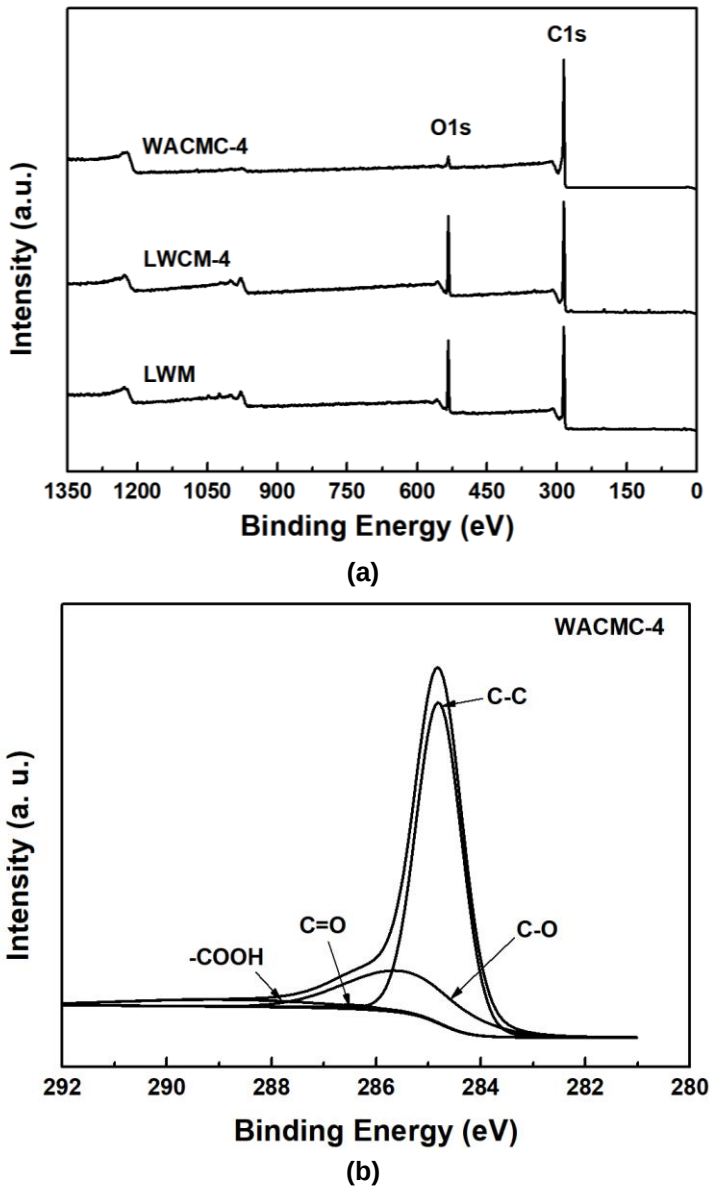

Fig. 4. XPS spectra of the LWM, LWCM-4, and WACMC-4 (a); and peak fitting of the XPS C1s peaks for WACMC-4 (b)

Table 1. Surface Elemental Composition of the LWM, LWCM-4, and WACMC-4

Sample	C1s (%)	O1s (%)	N1s (%)	O/C (%)
LWM	77.34	21.35	1.31	27.61
LWCM-4	77.24	21.63	1.04	28.00
WACMC-4	95.13	4.35	0.67	0.045

Table 2 summarizes the percentages of the graphitic and functional carbon atoms of the samples. The comparison of the spectra was done between LWM, LWCM-4, and WACMC-4. After chemical curing, the oxygen functional groups decreased, except for the carboxyl groups, which increased due to oxidation of the hydrochloric acid. After activation, the amount of graphitic carbon increased, whereas the carbonyl and carboxyl

groups were reduced, which was mainly because, under the conditions of high temperature and water steam, more graphitic carbons were enriched and reacted with steam water molecules to generate functional groups containing C-O (Lin and Zhao 2016). The carbonyl and carboxyl groups combusted, which resulted in volatile byproducts, such as CO_2, CO, H_2O, *etc*.

Table 2. Results of the Fits of the C1s Regions

Sample	C-C		C-O		C=O		-COOH	
	BE (eV)	RC* (%)	BE (eV)	RC (%)	BE (eV)	RC (%)	BE (eV)	RC (%)
LWM	284.7	58.66	285.5	18.88	286.5	20.63	288.3	1.83
LWCM-4	284.7	60.19	285.6	15.16	286.5	14.63	288.3	10.02
WACMC-4	284.8	70.10	285.5	22.19	286.4	1.07	288.9	6.64
*RC values given in % represent the relative content								

Pore Structure of the WACMCs

The N_2 adsorption-desorption isotherms of the WACMCs are shown in Fig. 5. The amount of adsorption in the low-pressure zone increased rapidly, which indicated that the samples had a typical microporous structure. The isotherms displayed hysteresis loops to various degrees, which indicated that there was part of an irregular mesopore structure inside of the samples (Jin and Huang 2015). As the hydrochloric acid concentration increased, the isotherms showed a more pronounced knee shape, which indicated that a mesoporous structure with a smaller pore size formed in the samples (Lee *et al*. 2003). Furthermore, the N_2 adsorption capacity of the WACMC-4 was the highest at 586 cm^3/g.

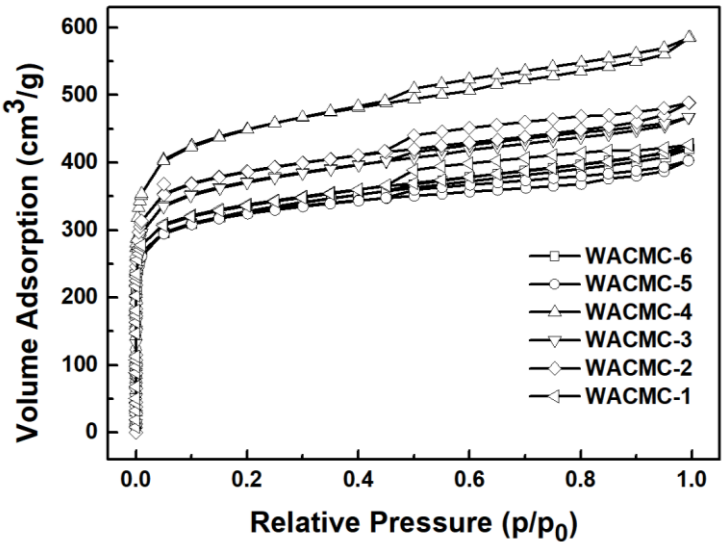

Fig. 5. N_2 adsorption-desorption isotherms of the WACMCs

Table 3 shows the nitrogen adsorption and pore structure parameters of the WACMCs. As the hydrochloric acid concentration increased from 1 mol/L to 6 mol/L, the specific surface area increased from 1290 m^2/g to a maximum of 1551 m^2/g at 4 mol/L, and then decreased to 1239 m^2/g.

Table 3. Nitrogen Adsorption and Pore Structure Parameters of the WACMCs

Sample	S_{BET} (m^2/g)	S_{micro} (m^2/g)	V_{micro} (cm^3/g)	S_{meso} (m^2/g)	V_{meso} (cm^3/g)	V_{total} (cm^3/g)
WACMC-6	1239	982	0.398	191	0.215	0.650
WACMC-5	1243	1061	0.427	138	0.172	0.624
WACMC-4	1511	1261	0.506	213	0.246	0.796
WACMC-3	1413	1155	0.465	195	0.211	0.723
WACMC-2	1386	1143	0.495	183	0.226	0.756
WACMC-1	1290	1054	0.421	176	0.204	0.660

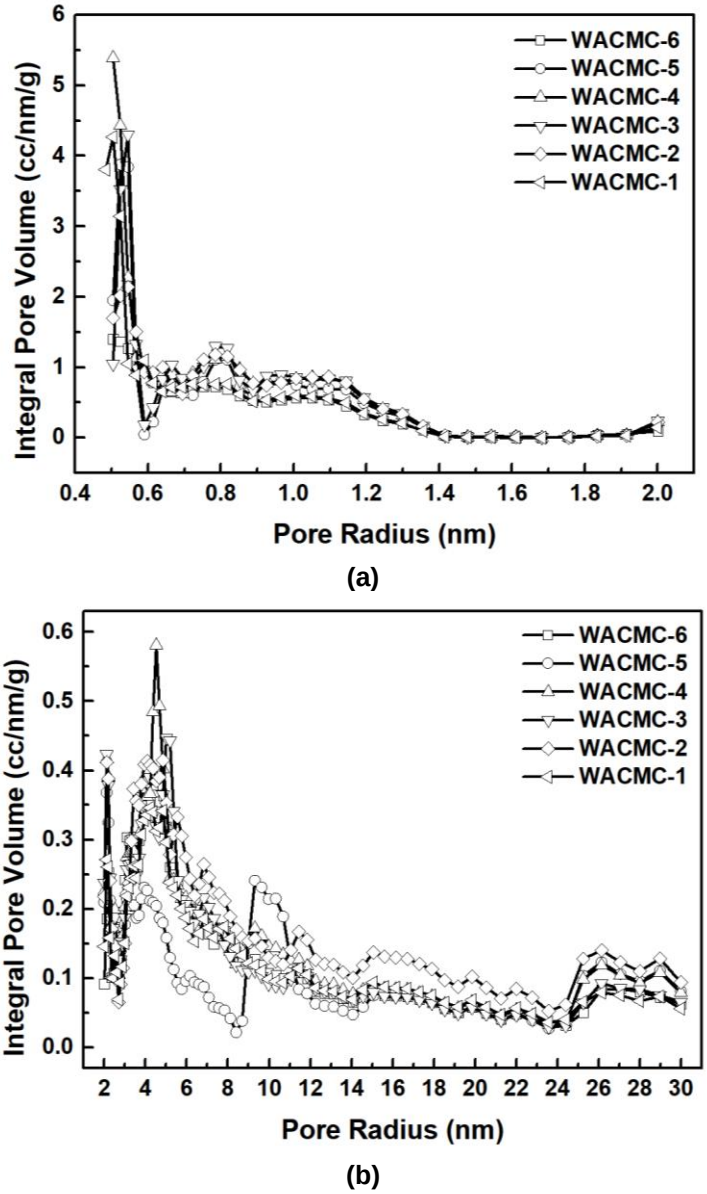

Fig. 6. Pore size distributions of the micropore (a) and mesopore (b) areas of the WACMCs

The same was true for the micropore and mesopore volumes. When the hydrochloric acid concentration was lower, the solidified layer on the surface was too weak and the internal cross-linking degree was not strong enough to protect the LWCMs from

the water steam, which meant that the pores were more likely to collapse during activation. This accounted for the nitrogen adsorption and pore structure parameters. In contrast, when the hydrochloric acid concentration was too high, a dense solidified layer formed quickly on the surface of the LWCMs, which hindered the entry of carbocations and resulted in a weak cross-linking degree inside of the precursors during the process of chemical curing. Therefore, the inner structure was vulnerable to collapse during activation when the water steam penetrated though the solidified layer into the cured microspheres.

Figure 6 shows the pore size distributions of the WACMCs. Figures 6a and 6b show the micropore and mesopore areas (2 nm to 30 nm), respectively. The pore size distribution of the micropore area was mainly concentrated to the range of 0.5 nm to 1.4 nm. In the mesopore region, the pore size distribution of the mesopores was mainly concentrated between 2 nm to 10 nm. The mesoporous structure with the smaller pore size distribution of the WACMCs was prepared by chemical curing and activation. Therefore, chemical curing contributed to the development of the specific surface area and pore volume of the WACMCs, but had little effect on the pore size distribution.

CONCLUSIONS

1. After chemical curing, the pyrolysis residual ratio of the liquefied wood microspheres (LWCMs) was improved obviously. As the hydrochloric acid concentrations increased, the pyrolysis residual ratio first increased to the highest at 51.3% (the hydrochloric acid concentration of 4 mol/L), then decreased. Moreover, the reaction between the carbocations and benzene rings contributed to the reinforcement of the intensity of methylene functional groups and cross-linking degree of the wood-based cured microspheres either.
2. The WACMCs had a typical microporous structure and formed part of an irregular mesoporous structure. The specific surface area, micropore volume, and mesopore volume increased at first and then decreased as the hydrochloric acid concentration increased from 1 mol/L to 6 mol/L. When the concentration was 4 mol/L, the specific surface area, micropore volume, and mesopore volume were 1551 m^2/g, 0.506 cm^3/g, and 0.246 cm^3/g, respectively. The pore size distribution of the micropore area was mainly concentrated to the range of 0.5 nm to 1.4 nm, and that of the mesopore area was mainly concentrated between 2 nm to 10 nm.

ACKNOWLEDGMENTS

The authors are grateful for the support of "The Fundamental Research Funds for the Central Universities" (Grant No. 2017PT11).

REFERENCES CITED

Azargohar, R., and Dalai, A. K. (2008). "Steam and KOH activation of biochar: Experimental and modeling studies," *Micropor. Mesopor. Mat.* 110(2-3), 413-421. DOI: 10.1016/j.micromeso.2007.06.047

Chiang, Y.-C., Lee, C.-C., and Lee, H.-C. (2007). "Characterization of microstructure and surface properties of heat-treated PAN-and rayon-based activated carbon fibers," *J. Porous Mat.* 14(2), 227-237. DOI: 10.1007/s10934-006-9028-8

De Boer, J. H., Lippens B. C., Linsen B. G., Broekhoff J. C. P., Van den Heuvel A., and Osinga T. J. (1966). "The T-curve of multimolecular N_2-adsorption," *J. Colloid Interf. Sci.* 21(4), 405-414. DOI: 10.1016/0095-8522(66)90006-7

Geng, J., Li, L.-F., Wang, W.-L., Chang, J.-M., Xia, C.-L., Cai, L.-P., and Shi, S. Q. (2017). "Fabrication of activated carbon using two-step co-pyrolysis of used rubber and larch sawdust," *BioResources* 12(4), 8641-8652. DOI: 10.15376/biores.12.4.8641-8652

Huang, Y., and Zhao, G. (2016). "A novel method for the production of mesoporous activated carbon fibers from liquefied wood," *Mater. Lett.* 178, 190-192. DOI: 10.1016/j.matlet.2016.03.064

Jin, Y. R., and Huang, Z. X. (2015). "Adsorption isotherms," in: *Adsorption and Pore Size Distribution*, *1st Ed.*, National Defense Industry Press, Beijing, China, pp. 87-105.

Lastoskie, C., Gubbins, K. E., and Quirke, N. (1993). "Pore size distribution analysis of microporous carbon: A density functional theory approach," *J. Phys. Chem.* 97(18), 4786-4796. DOI: 10.1021/j100120a035

Lee, Y.-S., Basova, Y. V., Edie, D. D., Reid, L. K., Newcombe, S. R., and Ryu, S.-K. (2003). "Preparation and characterization of trilobal activated carbon fibers," *Carbon* 41(13), 2573-2584. DOI: 10.1016/S0008-6223(03)00376-2

Li, D., and Ma, X. (2013). "Preparation and characterization of activated carbon fibers from liquefied wood," *Cellulose* 20(4), 1649-1656. DOI: 10.1007/s10570-013-9981-8

Lin, J., and Zhao, G. (2016). "Preparation and characterization of high surface area activated carbon fibers from lignin," *Polymers-Basel* 8(10), 369-378. DOI: 10.3390/polym8100369

Lin, J., Kubo, S., Yamada, T., Koda, K., and Uraki, Y. (2012). "Chemical thermostabilization for the preparation of carbon fibers from softwood lignin," *BioResources* 7(4), 5634-5646. DOI: 10.15376/biores.7.4.5634-5646

Lin, J., Shang, J.-B., and Zhao, G.-J. (2013). "The preparation and characterization of liquefied wood based primary fibers," *Carbohyd. Polym.* 91(1), 224-228. DOI: 10.1016/j.carbpol.2012.08.007

Liu, W., and Zhao, G. (2012). "Effect of temperature and time on microstructure and surface functional groups of activated carbon fibers prepared from liquefied wood," *BioResources* 7(4), 5552-5567. DOI: 10.15376/biores.7.4.5552-5567

Liu, W., Zhang, Q., and Zhao, G. (2015). "Influence of activation time on the microstructure and antibacterial activity of nanosilver-containing activated carbon fibers prepared from liquefied wood," *Fiber. Polym.* 16(3), 522-528. DOI: 10.1007/s12221-015-0522-y

Ma, X., and Zhao, G. (2008). "Structure and performance of fibers prepared from liquefied wood in phenol," *Fiber. Polym.* 9(4), 405-409. DOI: 10.1007/s12221-008-0065-6

Ma, X., and Zhao, G. (2010). "Preparation of carbon fibers from liquefied wood," *Wood Sci. Technol.* 44(1), 3-11. DOI: 10.1007/s00226-009-0264-3

Ma, X., and Zhao, G. (2011). "Variations in the microstructure of carbon fibers prepared from liquefied wood during carbonization," *J. Appl. Polym. Sci.* 121(6), 3525-3530. DOI: 10.1002/app.34142

Ma, X. J., Yang, H. M., Yu, L. L., Chen, Y., and Li, Y. (2014). "Preparation, surface and pore structure of high surface area activated carbon fibers from bamboo by steam activation," *Materials* 7(6), 4431-4441. DOI: 10.3390/ma7064431

Mangun, C. L., Benak, K. R., Economy, J., and Foster, K. L. (2001). "Surface chemistry, pore sizes and adsorption properties of activated carbon fibers and precursors treated with ammonia," *Carbon* 39(12), 1809-1820. DOI: 10.1016/S0008-6223(00)00319-5

Neimarka, A. V., Lin, Y. Z., Ravikovitch, P. I., and Thommes, M. (2009). "Quenched solid density functional theory and pore size analysis of micro-mesoporous carbons," *Carbon* 47(7), 1617-1628. DOI: 10.1016/j.carbon.2009.01.050

Okada, K., Yamamoto, N., Kameshima, Y., and Yasumori, A. (2003). "Porous properties of activated carbons from waste newspaper prepared by chemical and physical activation," *J. Colloid Interf. Sci.* 262(1), 179-193. DOI: 10.1016/S0021-9797(03)00107-3

Shang, J., Lin, J., Zhao, G., Zhang, J., Su, Z., and Guo, S. (2015). "Effects of time and chemical curing temperature on the properties of liquefied wood-based precursors and carbon fibers," *BioResources* 10(4), 7477-7488. DOI: 10.15376/biores.10.4.7477-7488

Shen, Z. M., Zhang, W. H., and Zhang, X. J. (2008). "Activated carbon microspheres" in: *Preparation and Application of Activated Carbon Materials, (1st ed.)*, Chemical Industry Press, Beijing, China, pp. 127-131.

Valente Nabais, J. M., Carrott, P. J. M., Ribeiro Carrott, M. M. L., and Menéndez, J. A. (2004). "Preparation and modification of activated carbon fibres by microwave heating," *Carbon* 42(7), 1315-1320. DOI: 10.1016/j.carbon.2004.01.033

Wang, H., Shi, L., Yan, T., Zhang, J., Zhong, Q., and Zhang, D. (2014). "Design of graphene-coated hollow mesoporous carbon spheres as high performance electrodes for capacitive deionization," *J. Mater. Chem. A* 2(13), 4739-4750. DOI: 10.1039/C3TA15152B

Wang, Y., Yang, R., Li, M., and Zhao, Z. (2015). "Hydrothermal preparation of highly porous carbon spheres from hemp (*Cannabis sativa* L.) stem hemicellulose for use in energy-related applications," *Ind. Crop. Prod.* 65, 216-226. DOI: 10.1016/j.indcrop.2014.12.008

Wickramaratne, N. P., and Jaroniec, M. (2013). "Importance of small micropores in CO_2 capture by phenolic resin-based activated carbon spheres," *J. Mater. Chem. A* 1(1), 112-116. DOI: 10.1039/C2TA00388K

Ye, C., Gong, Q.-M., Lu, F.-P., and Liang, J. (2008). "Preparation of carbon nanotubes/phenolic-resin-derived activated carbon spheres for the removal of middle molecular weight toxins," *Sep. Purif. Technol.* 61(1), 9-14. DOI: 10.1016/j.seppur.2007.09.021

Zhang, T., and Shen, Q. (2009). "Preparation and characterization of carbon fiber derived from lignin-phenol-formaldehyde resin," *Journal of Cellulose Science and Technology* 17(2), 6-11. DOI: 10.3969/j.issn.1004-8405.2009.02.002

Article submitted: May 4, 2018; Peer review completed: July 21, 2018; Revised version received: July 25, 2018; Accepted: July 27, 2018; Published: August 1, 2018.
DOI: 10.15376/biores.13.4.7175-7187